Interaction Forces between F-Actin and Titin PEVK Domain Measured with Optical Tweezers

Pasquale Bianco,* Attila Nagy, András Kengyel, Dávid Szatmári, Zsolt Mártonfalvi, Tamás Huber, and Miklós S. Z. Kellermayer
*Department of Biophysics, University of Pécs, Faculty of Medicine, Pécs H-7624 Hungary

ABSTRACT Titin is a giant protein that determines the elasticity of striated muscle and is thought to play important roles in numerous regulatory processes. Previous studies have shown that titin's PEVK domain interacts with F-actin, thereby creating viscous forces of unknown magnitude that may modulate muscle contraction. Here we measured, with optical tweezers, the forces necessary to dissociate F-actin from individual molecules of recombinant PEVK fragments rich either in polyE or PPAK motifs. Rupture forces at a stretch rate of 250 nm/s displayed a wide, nonnormal distribution with a peak at ~8 pN in the case of both fragments. Dynamic force spectroscopy experiments revealed low spontaneous off-rates that were increased even by low forces. The loading-rate dependence of rupture force was biphasic for polyE in contrast with the monophasic response observed for PPAK. Analysis of the molecular lengths at which rupture occurred indicated that there are numerous actin-binding regions along the PEVK fragments' contour, suggesting that the PEVK domain is a promiscuous actin-binding partner. The complexity of PEVK-actin interaction points to an adaptable viscoelastic mechanism that safeguards sarcomeric structural integrity in the relaxed state and modulates thixotropic behavior during contraction.

INTRODUCTION

Titin is a giant filamentous protein that determines muscle elasticity and, via its different domains and associated proteins, is thought to play key roles in important regulatory processes (1,2). In the functionally extensible I-band section of titin, a unique proline-, glutamate-, valine- and lysine-rich (PEVK) domain is present (3). Titin isoforms with different lengths and PEVK-domain sizes are expressed in different muscle types (3,4). PEVK is thought to acquire a random, intrinsically disordered structure as a result of the preponderance of highly charged residues (3,5). Immunoelectron microscopic analysis has shown that the PEVK domain indeed behaves as a quasiunfolded, random protein chain (6). Structural experiments suggested that the PEVK domain may contain left-handed polyproline helices (7). From sequence analysis, a repetitive motif structure was discovered in PEVK (8,9). Two main motifs have been identified (8): PPAK and polyE. PPAK motifs are ~28-residue-long sequences that begin most often with the amino acids PPAK. PolyE motifs contain a preponderance of glutamate. Recently the PEVK domain was suggested to be a malleable structure capable of transition among various conformational states (10).

Titin's PEVK domain has been shown in several works to bind F-actin. An interaction between cardiac PEVK and F-actin has been found (11,12), and the binding could be modulated by Ca^{2+}/S100 (13). Human fetal skeletal PEVK was shown to interact with thin-filament proteins (actin, nebulin) (9). Recently we have shown that the PEVK domain of the full-length skeletal-muscle (soleus) titin isoform binds actin along its entire length, but with different apparent local affinities (14). We hypothesized that the PEVK–F-actin interaction might function as a viscous bumper that regulates the velocity of sarcomeric shortening. More recent observations support the possibility that PEVK-actin interaction may play a regulatory role in muscle contraction (15,16). However, the actin-binding site(s) along the PEVK domain, the dynamics of the PEVK-actin bond, and the forces involved in modulating the interaction have remained unknown.

In this work we explored, by using force-measuring optical tweezers, the mechanics and dynamics of the interaction between F-actin and recombinant skeletal-muscle PEVK fragments. The bonds can be broken with relatively low (~8 pN) forces. Calculated spontaneous off-rates of the PEVK–F-actin bonds are low, suggesting a structure-maintaining role rather than a regulatory function. The lack of canonical actin-binding sites and the multiplicity of actin-binding spots along the fragments indicate that the PEVK domain may be a promiscuous actin-binding partner. The complexity of PEVK-actin interaction points to an adaptable viscoelastic mechanism that safeguards against sarcomeric structural rearrangement in relaxed muscle and determines the thixotropic properties of muscle.

MATERIALS AND METHODS

Cloning, expression, and purification of proteins

PEVK fragments were cloned, expressed, and purified as previously described (14). The fragments used in the work presented here were the

Submitted February 7, 2007, and accepted for publication May 11, 2007.

Address reprint requests to Miklós S. Z. Kellermayer, Dept. of Biophysics, University of Pécs, Faculty of Medicine, Szigeti út 12, Pécs H-7624 Hungary. Tel.: 36-72-536-271; Fax: 36-72-536-261; E-mail: miklos.kellermayer.jr@aok.pte.hu.

Pasquale Bianco's permanent address is Laboratorio di Fisiologia, DBAG, Dipartimento di Fisica, Polo Scientifico, I-50019 Sesto Fiorentino (FI), Italy.

Editor: Shin'ichi Ishiwata.

0006-3495/07/09/2102/08 $2.00

doi: 10.1529/biophysj.107.106153

following: 1), PEVKII, the middle one-third of the soleus-isoform PEVK domain (residue boundaries 6359–7064, GenBank accession No. X90569, version X90569.1); 2), PPAK, a fragment rich in PPAK motifs (residue boundaries 5805–6005); and 3), polyE, a fragment containing only polyE motifs (a tandem doublet of the 6769–6840 residue sequence separated by an *Eco*RI cleavage site). To the C-terminus of the fragments two vicinal cysteines were added for subsequent mechanical handling. His_6-tagged (on N-terminus) proteins expressed in *E. coli* (BL21(DE3)pLysS) were purified on Ni^{2+}-NTA columns (Qiagen, Valencia, CA) under native conditions and further purified on a Sephadex G-25 column. The molecular handles added a total 25 residues to each of the fragments. Actin (17), myosin (18), and heavy meromyosin (HMM) (19) were purified according to established methods. For stabilization against depolymerization and for fluorescence imaging, F-actin was labeled with a molar excess of tetramethylrhodamine-isothiocyanate-phalloidin (TRITC-phalloidin, Molecular Probes, Eugene, OR).

Preparation of functionalized microscopic beads

PEVK fragments were first biotinylated on their C-terminus (EZ-Link Maleimide PEO2-Biotin, Pierce, Rockford, IL). Subsequently, streptavidin-coated 3.1-μm-diameter latex beads (Spherotech) were coated with biotinylated PEVK fragments at a nominal density of ~200–1000 molecules per bead (Fig. 1 *a*).

F-actin was attached to carboxylated beads that had been precoated with HMM by cross-linking with carbodiimide. Actin filaments were first sonicated and then attached to the HMM-coated beads in rigor (absence of ATP) (Fig. 1 *b*). Fluorescence microscopic analysis has shown that the length of the sonicated actin filaments was ≤ 1 μm. To remove unbound actin filaments, the bead suspension was allowed to sediment for 1 h on ice, the supernatant was decanted, and the pellet gently resuspended in AB buffer (25 mM MOPS, pH 7.4, 4 mM $MgCl_2$, 0.01% NaN_3, 0.2% Tween-20, 1 mM dithiothreitol (DTT), 0.5 mg/ml bovine serum albumin (BSA)) containing 25 mM KCl. The procedure was repeated twice. The attachment of TRITC-phalloidin-labeled F-actin to the beads was checked with confocal microscopy. In some control experiments F-actin was directly attached to carboxylated beads by cross-linking with carbodiimide.

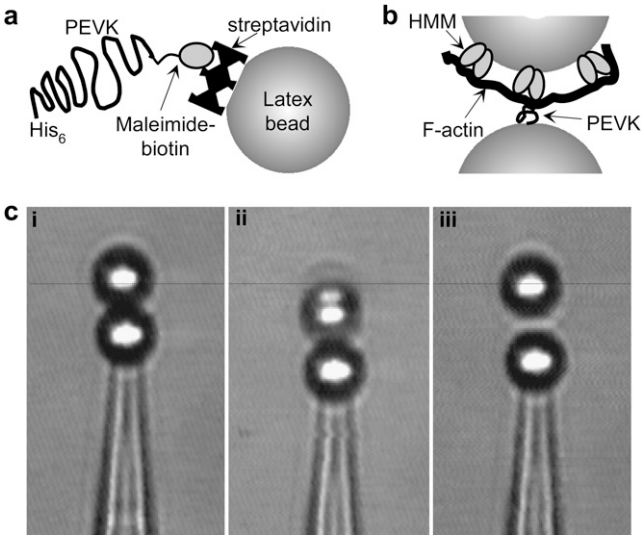

FIGURE 1 Experimental strategies for measuring interaction forces between PEVK and F-actin. (*a*) PEVK fragments were attached to the surface of streptavidin-coated latex beads via their C-terminally located cysteine residue using maleimide-biotin cross-linking. (*b*) Actin filaments were attached via rigor bonds to latex beads precoated with HMM. (*c*) Image sequence of the experimental procedure for measuring interaction forces. Upper bead is the actin-coated bead in the optical trap. Lower bead is the PEVK-fragment-coated bead held with a moveable glass micropipette. The beads were first pressed together (*i*), then pulled apart (*ii*) until a rupture event occurred followed by the sudden return of the upper bead to its equilibrium position in the trap center (*dotted line*) (*iii*).

To examine binding mechanisms and ensure single-molecule interactions, the probabilities of forming interaction between a PEVK-fragment-coated and an actin-coated bead were compared with the predictions of Poisson statistics (20–22). To assay for binding probability, a bead coated with PEVK fragment (PPAK or polyE) at different densities was pressed against a bead coated with F-actin. The mean pushing force and duration were ~35 pN and ~6 s, respectively. Five hundred binding attempts were assayed at each coating density. Nominal coating densities were 200, 400, 600, and 1000 molecules per bead. Binding probability was expressed as the ratio of the number of successful binding events per total number of binding attempts.

Optical tweezers

Interaction forces between PEVK and F-actin were measured with a dual-beam counterpropagating optical tweezers apparatus (23–25). Briefly, two beams from single-mode diode lasers (200 mW CW, 833 nm, JDS-Uniphase, Milpitas, CA) were directed with dichroic mirrors into two microscope objectives facing each other (60×, 1.2 NA water immersion, Olympus Hungary, Budapest), which focused the beams to the same spot in a flow-through microchamber positioned, with a low-profile closed-loop *XYZ* piezoelectric stage (Mad City Labs, Madison, WI) between the objectives. The beams partially filled the back aperture of the objectives so that the photons leaving the trap were efficiently collected with the opposite objective lens. The objective back aperture was refocused onto position-sensing photodiodes (UDT, San Diego, CA). Force was measured by calculating the change in light momentum (25). Trap stiffness and maximal force were ~0.1 pN/nm and ~150 pN, respectively. The flow-through microchamber was custom made from two microscope coverslips (24 × 60 mm) and two parafilm spacers. A narrow micropipette (1 μm tip diameter) was inserted in the microchamber for the capture and handling of microscopic beads. The microchamber was mounted on the *XYZ* piezoelectric stage; therefore, the movement of the micropipette, and hence the bead captured by it, was carried out by positioning the entire flow chamber. Brightfield microscopic images of the beads and micropipette, illuminated with an arc-lamp (Fiber-Lite, WPI Germany, Berlin), were detected using a ¾-inch CCD camera (Tokyo Instruments, Tokyo, Japan). Instrument control and data acquisition were carried out by using custom-written LabView algorithms.

PEVK-actin interaction forces were measured by first pressing together (for 5–9 s) then pulling apart the PEVK fragment- and F-actin-coated beads (Fig. 1 *c*). The pipette bead was pulled away from the trap with a constant velocity (varied between 100-5000 nm/s). The force in the instant of the rupture of the connection between the two beads was measured. The assay was carried out at room temperature in AB buffer containing 150 mM KCl. In ionic-strength-dependent assays, the KCl concentration was varied between 25 and 250 mM.

Statistics and analysis

Rupture events were identified in the force-versus-time plots as a gradual rise in force followed by sudden force drop. Loading rate (r) was calculated from trap stiffness (κ) and stretch rate (v) as

$$r = \kappa v. \quad (1)$$

In case of elastic tethers, the loading rate was calculated by fitting a line to the rising phase of the force trace immediately preceding the rupture event. Loading-rate deviations caused by elastic tethers were indicated as horizontal error bars in the rupture force versus loading rate plot (see Fig. 4 *d*). Bond rupture forces (F_r) are related to the kinetics of PEVK-actin dissociation as

$$F_r = \frac{k_B T}{x_\beta} \ln\left(\frac{r x_\beta}{k_{off}^0 k_B T}\right), \quad (2)$$

where k_{off}^0 is the spontaneous off-rate, x_β is the distance between bound and transition states along the reaction coordinate, r is loading rate, k_B is Boltzmann's constant, and T is absolute temperature (26,27). The kinetic parameters (k_{off}^0 and x_β) were obtained by fitting Eq. 2 on the experimentally obtained rupture force versus loading rate data.

To obtain polymer mechanical parameters of PEVK tethers, nonlinear force (F) versus extension (z) curves were fitted with the wormlike chain (WLC) model of entropic elasticity (28),

$$\frac{FA}{k_B T} = \frac{z}{L} + \frac{1}{4(1 - z/L)^2} - \frac{1}{4}, \quad (3)$$

where A is persistence length, and L is contour length (tether length).

To distinguish between binding mechanisms, binding probability data were fitted with equations for Poisson probabilities for the cases of single-molecule binding

$$P(d) = 1 - e^{-\lambda d} \quad (4)$$

and double-molecule binding

$$P(d) = 1 - e^{-\lambda d} - \lambda d e^{-\lambda d}, \quad (5)$$

where $P(d)$ is binding probability at coating density d, and λ is a fitting paramenter (22). For calculations and statistical analyses, we used IgorPro (v. 5.0), KaleidaGraph (v. 4.0), and Microcal Origin (v. 6.0) software packages.

RESULTS

Measurement of PEVK-fragment–F-actin interaction forces

The forces necessary to rupture the interaction between the PEVK domain of titin and F-actin were measured with optical tweezers. We used the recombinant fragments ''PEVKII'', ''PPAK'', and ''polyE'' of the PEVK domain, all of which had previously been shown to bind F-actin (14).

To measure the mechanical strength of the PEVK-actin interaction, a PEVK-fragment-coated latex bead (Fig. 1 *a*), held with a moveable micropipette, was pressed against then pulled away from a latex bead, held in an optical trap, onto which actin filaments were attached. To mimic sarcomeric geometry as nearly as possible, actin filaments were attached to heavy-meromyosin (HMM)-coated beads via rigor bonds (Fig. 1 *b*). The beads were then pulled apart by moving the micropipette away from the trap (Fig. 1 *c*), thereby loading the bond(s) connecting PEVK and actin, and force was monitored as a function of time. Typical force-versus-time traces obtained in PEVKII-actin interaction force spectroscopy experiments are shown in Fig. 2 *a*. Positive forces correspond to interaction forces, and negative forces to compression forces with which the beads were pressed together. In the force spectrum sawtooth-shaped peaks can be observed that consist of a rising slope, a peak and a rapid force drop. Force rises during stretch because interactions formed between actin and PEVK during the compression period hold the beads together. Sometimes we observed nonlinearity during the rising phase of the sawtooth, suggesting that a tether with a certain length connected the beads (see Fig. 2 *g*). The peak corresponds to the force at the instant of the rupture of PEVK-actin interaction. This rupture force, which is an important parameter of the mechanical properties of the PEVK-actin interaction, was measured under various experimental conditions. To test whether the observed force spectra indeed arise from PEVK-actin interaction, we carried out several control experiments. When a PEVKII-coated bead was pressed against either an HMM- (Fig. 2 *b*) or a BSA-coated bead (Fig. 2 *c*), or when an F-actin-coated bead was pressed against a BSA-coated bead (Fig. 2 *d*), we observed no interactions. To test whether rupture forces might arise from the breakage of the acto-HMM rigor bond, we measured the interaction forces between PEVKII-coated beads

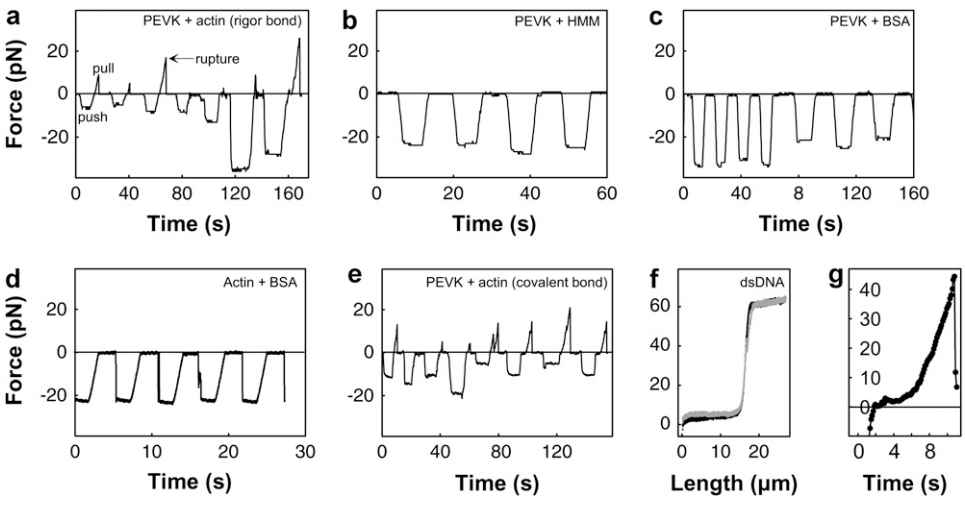

FIGURE 2 Collection of force traces obtained in PEVK-actin interaction and control experiments. (*a*) Time-dependent force trace of interaction between a bead coated with PEVKII and a bead coated with acto-HMM (*rigor bond*). Results of control experiments between beads coated with PEVKII and HMM (*b*), PEVKII and BSA (*c*), and actin and BSA (*d*), respectively. (*e*) Force trace of interaction between a bead coated with PEVKII and a bead with covalently linked actin. (*f*) Force-versus-extension curve of a λ-phage DNA molecule linked to streptavidin-coated beads via its biotinylated ends. Stretch rate 250 nm/s. Solid and shaded traces correspond to stretch and relaxation data, respectively. (*g*) Example of a force-versus-time trace for PEVKII and F-actin interaction in which nonlinear behavior can be seen.

and beads that were directly coated with F-actin using a covalent cross-linker (Fig. 2 *e*). The results were indistinguishable from those obtained for HMM-actin-coated beads. Finally, to test whether the observed rupture events might be caused by the dissociation of the streptavidin-biotin bond, we stretched a λ-phage DNA molecule biotinylated at its ends and attached to streptavidin-coated beads (Fig. 2 *f*). We found no rupture events at forces above 60 pN, which far exceed the range of forces in which the PEVK-actin rupture events were observed.

Effect of ionic strength

To test the mechanisms of PEVK-actin interaction and whether the interaction occurs at physiological ionic strengths, mechanical measurements were carried out at increasing KCl concentrations (Fig. 3). We measured the success rate of forming bead-bead interaction as a function of ionic strength. Success rate, defined as the ratio of the number of successful bead engagement attempts that resulted in rupture forces versus the number of total bead engagement attempts, was constant across the ionic strength range of 25–150 mM. Above 150 mM, the success rate dropped sharply, and essentially no PEVK-actin interaction could be observed at ionic strengths above 250 mM. Subsequent experiments were carried out at 150 mM KCl.

PEVK-actin rupture force statistics

Fig. 4 *a* shows the distribution of rupture forces for PEVKII at a mean stretch rate of 250 nm/s. A wide distribution of rupture forces can be observed with a major peak at ~6 pN and local modes at higher forces. To dissect the interaction further, motif-rich PEVK fragments were examined. Fig. 4, *b* and *c*, shows the distribution of rupture forces for polyE and PPAK fragments for different stretch rates. At a stretch rate of 250 nm/s, a relatively wide distribution is observed, with rupture forces ranging from 2 to 35 pN and a peak at ~8 pN. Increasing the stretch rate to 5000 nm/s resulted in increased mean rupture force and widened rupture force range. To test whether the wide range of forces is caused by the interaction of multiple PEVK molecules with the actin-coated bead, we systematically reduced the density of PPAK fragments on the bead surface and carried out dynamic force spectroscopy measurements (Fig. 4 *d*). Although reduction of the nominal bead coating density (calculated as total PEVK concentration per total bead concentration) from 1000 to 400 molecules/bead reduced the mean rupture force, there was no significant difference in rupture forces between 400 and 200 PPAK molecules/bead. The success rate of finding bead-bead interaction became low in the case of 200 PEVK molecules/bead. Further dilution resulted in extremely rare binding events. Therefore, subsequent measurements were carried out at a nominal coating density of 200 molecules/bead.

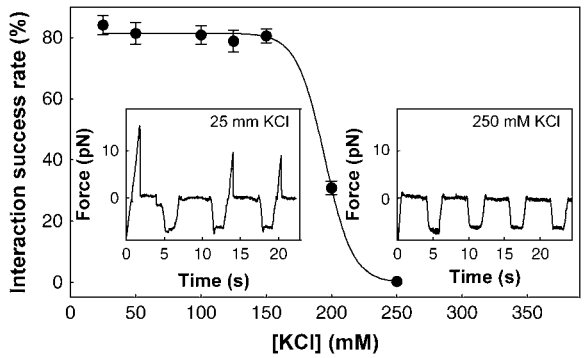

FIGURE 3 Effect of ionic strength on actin-PEVKII interaction. Interaction success rate as a function of KCl concentration, calculated as the number of rupture events per the total number of interaction trials. Force-versus-time trace for an experiment at 25 mM KCl (*left inset*) and 250 mM KCl (*right inset*). Nominal bead coating density ~1000 molecules/bead.

Apparent kinetic parameters of the PEVK-actin interaction were obtained by measuring rupture force as a function of loading rate (Fig. 4 *e*). The loading-rate-dependent rupture force relationship was better fitted with two independent functions (Eq. 2) in the case of polyE. By contrast, a single function gave good fit in the case of the PPAK fragment. For the polyE–F-actin interaction at low loading rates (<100 $pN \cdot s^{-1}$), the spontaneous off-rate (k_{off}^0) and the unbinding potential width (x_β) were $0.004 \pm 0.003\ s^{-1}$ and 1.21 ± 0.13 nm, respectively. At high loading rates (>100 $pN \cdot s^{-1}$), k_{off}^0 and x_β were $0.406 \pm 0.074\ s^{-1}$ and 0.42 ± 0.02 nm, respectively. For the PPAK–F-actin interation, k_{off}^0 and x_β were $0.135 \pm 0.017\ s^{-1}$ and 0.58 ± 0.02 nm, respectively.

To substantiate the singularity of molecular interactions between PEVK fragments and F-actin, the binding probabilities were plotted against the nominal bead coating density (Fig. 4 *f*) and compared with Poisson statistics (20–22). We obtained good fit for single-molecule binding mechanism (Eq. 4, $\chi^2 = 0.002$) for both polyE and PPAK fragments. By contrast, the equation for double-molecule binding (Eq. 5) gave a poorer fit ($\chi^2 = 0.01$). The analysis also indicated that at the nominal bead coating density of 200 molecules per bead, the probability of simultaneous binding of two PEVK fragment molecules to the actin-coated bead was extremely low (0.006).

Geometry of PEVK–F-actin interaction

In many cases (~60% of the binding events for polyE and PPAK), we observed that the rupture occurred at a length-offset, suggesting that a tether was formed between the two beads (Fig. 5, *a* and *b*). In these experiments the rupture event was preceded by a nonlinear curve in the force-versus-length trace. In the case of long tether lengths, the nonlinear rising part of the force trace was often preceded by a flat trace at near-zero forces. The tether-length (contour length of WLC fit) histogram could be fitted with a sigmoid function

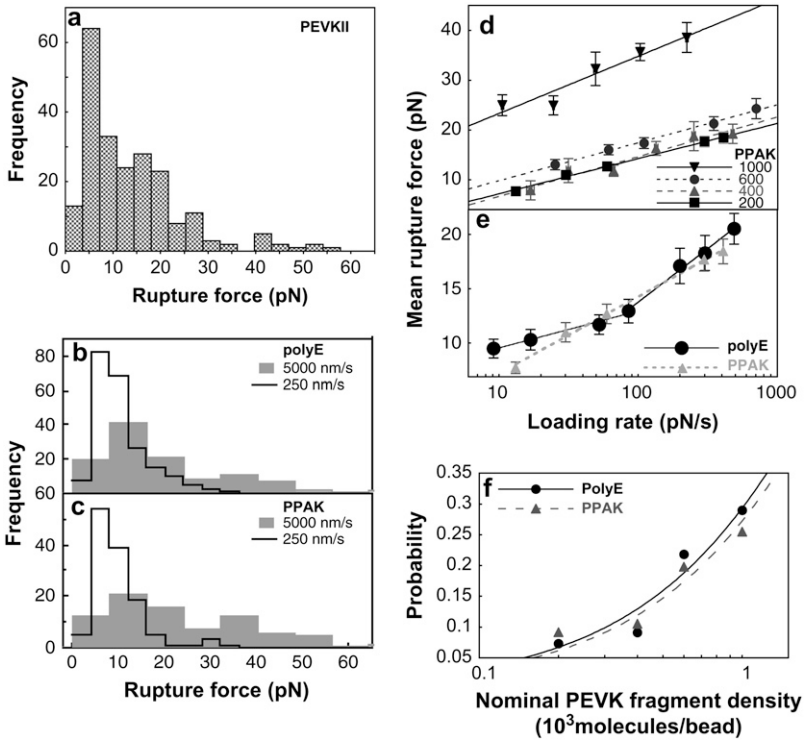

FIGURE 4 Force spectroscopy results. (*a*) Distribution of rupture forces for PEVKII–F-actin interaction. (*b*) PolyE fragment–F-actin and (*c*) PPAK–F-actin rupture-force histograms for high (5000 nm/s, *shaded bar*) and low (250 nm/s, *solid line*) stretch rates, respectively. (*d*) Mean PPAK fragment–F-actin rupture force as a function of loading rate for different bead coating densities (~200–1000 molecules/bead). Horizontal error bars describe the deviation in loading rate caused by elastic tethers (see Materials and Methods). (*e*) Mean polyE fragment and F-actin rupture force as a function of loading rate in comparison with that of PPAK fragment. Nominal coating density ~200 molecules/bead. (*f*) Probability of binding between a PEVK-fragment-coated bead and an actin-coated bead as a function of coating density. Fits were made using Poisson probability equation for single-molecule binding mechanism (Eq. 4).

in the case of the polyE fragment (Fig. 5 *c*), suggesting that the actin-binding sites are distributed along its entire calculated ~65-nm length (171 residues × 0.38 nm spacing) and that these sites are more-or-less equally accessible. In support of this notion, we sometimes observed plateaus in the force-versus-length traces (Fig. 5 *c*, *inset*) that likely correspond to the breakage of consecutive interactions in an unzipping process. The length histogram could be fitted with a single exponential function in the case of the PPAK fragment (Fig. 5 *d*). The frequency of rupture events became minimal at lengths exceeding the calculated ~86-nm length of the PPAK fragment (226 residues × 0.38 nm). In the case of the ~278-nm-long PEVKII fragment (731 residues × 0.38 nm), multiple plateaus and rupture events were seen in force-versus-length plots (Fig. 5 *e*). In stretch-and-hold experiments (Fig. 5 *f*), we observed stress-relaxation where force decreased in discrete steps as a function of time.

DISCUSSION

Nanomechanics of PEVK-actin interaction

A viscous force of unknown magnitude has been speculated in recent years to arise in the sarcomere as a result of interaction between titin's PEVK domain and actin (12,14). In the work presented here we explored the nanomechanical features of the interaction between F-actin and PEVK fragments by using optical tweezers. We investigated a fragment rich in PPAK motifs (''PPAK fragment'') and another consisting entirely of polyE motifs (''polyE fragment'').

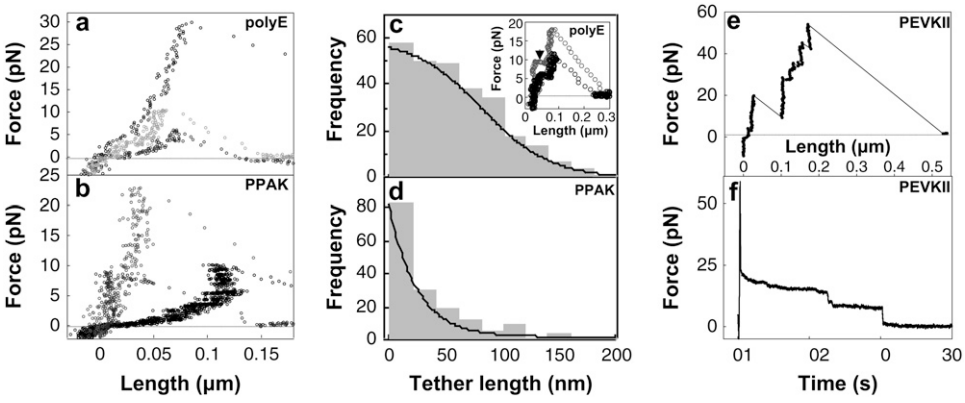

FIGURE 5 Examples of force-versus-length data for polyE (*a*) and PPAK (*b*) fragment and F-actin unbinding experiments in which tether length was evident. (*c*) Frequency of tether length for polyE. (*Inset*) Examples of force-versus-length curves with plateaus (*arrowhead*). (*d*) Frequency of tether length for PPAK. (*e*) Example of force-versus-length data for a PEVKII and F-actin unbinding experiment with appreciable tether length and multiple rupture events. (*f*) Stress relaxation in PEVKII and F-actin complex. The actin-coated bead was pulled away rapidly from the trapped PEVKII-coated bead and held in a fixed position; then force was monitored as a function of time.

PPAK and polyE represent the two main sequence motifs present in the PEVK domain (8). In addition, we measured interaction forces for a PEVK segment (''PEVKII'') that represents the middle of the PEVK domain of the soleus-muscle titin isoform (14).

Because both F-actin and the PEVK fragments are filamentous structures, the geometry of their arrangement is likely to influence their interaction. Actin filaments were mounted on beads densely precoated with HMM. In this arrangement the actin filaments, held with multiple rigor bonds on the HMM-coated bead, displayed their side toward the bead coated with the PEVK fragment. Although this molecular arrangement may not represent the usual physiological state when the molecular species interact (rigor versus relaxed state), it captures essential features of the sarcomeric arrangement of the filaments. Each of the PEVK fragments was captured via its biotinylated C-terminal end onto streptavidin-coated beads. The rest of the fragment molecule was therefore accessible for actin binding as much as its conformation and fluctuations permitted the process to take place. The loading direction was normal to the actin-filament axis. Although this geometry differs from that in the sarcomere, it allowed the probing of individual PEVK-actin interactions. Had the filaments been pulled in a direction parallel with their axis, the interconnecting bonds would have been loaded at the same time.

Although a complex set of molecules and interactions were involved, control experiments demonstrated that we were able to specifically identify and explore the interaction between the PEVK fragments and F-actin (Fig. 2). We excluded the possibility that either PEVK-HMM, PEVK-BSA, actin-BSA, biotin-streptavidin, or actin-HMM interaction contributed to our findings. Although individual actin-HMM rigor bonds can be broken with relatively low forces such as observed in this work (29), it is unlikely that the observed data resulted from the rupture of rigor bonds for several reasons: 1), actin filaments are coupled to multiple HMM molecules on the bead surface; 2), the kinetic parameters of the observed interactions (see Fig. 4) are different from that of the acto-HMM bond (29); and 3), replacing the acto-HMM-coated beads with ones carrying covalently coupled F-actin gave identical results (Fig. 2 *e*). Finally, it is highly unlikely that the observed rupture events are related to the breakage of the actin filament itself. Mechanical breakage of torsion-free actin filaments requires forces up to 600 pN (30).

Characteristics of the PEVK-actin bond

The properties of PEVK-actin interaction were characterized in several series of experiments. Increasing the KCl concentration above 150 mM abolished the formation of PEVK-actin bonds, suggesting that the interaction is electrostatic. Our results support previous observations (12,14) and indicate that the interaction occurs at physiologically relevant ionic strengths. Thus, in addition to its apparent elastic properties (31,32), the interactions of the PEVK domain might also be tuned by ionic conditions.

PEVK-actin rupture force histograms displayed a wide, nonnormal distribution (Fig. 4, *a–c*). At low stretch rates, a peak rupture force of ~8 pN was observed for both polyE and PPAK (Fig. 4, *b* and *c*). At high stretch rates, the rupture-force distribution broadened, and the peak (and mean) rupture force increased. To exclude the possibility that multiple PEVK fragment molecules are involved in the interactions, we systematically reduced the bead-surface density of the fragments. From comparisons with Poisson statistics (Fig. 4 *f*) we may conclude that single PEVK fragment molecules are able to bind an actin filament. Furthermore, at the 200 molecules per bead coating density, the simultaneous binding of two PEVK fragment molecules to the actin-coated bead was highly unlikely. Although the average rupture forces decreased with lowering of the bead coating density, the distribution of forces remained nonnormal. It is likely that although single PEVK fragment molecules took part in the interaction, several actin-binding sites along the fragment could be involved. Further experiments on tether-length distribution (Fig. 5) supported this idea.

The loading-rate dependence of rupture force was different for polyE and PPAK fragments (Fig. 4 *e*). Whereas in the case of PPAK a single function fitted the results, two different functions gave a good fit for polyE. We envision two possible scenarios to explain the biphasic loading-rate dependent rupture forces of the polyE fragment. One possibility is that the polyE–F-actin bond has a complex energy landscape involving an intermediate state (33). Another possibility is that multiple actin-binding sites along the polyE fragment with different kinetic parameters are involved. A similar biphasic distribution of bond lifetimes has been observed for the interaction between F-actin and the two-headed HMM molecule (29). Measurement of tether lengths (Fig. 5) revealed that there are indeed multiple actin-binding sites along the PEVK fragments. Further experimentation will reveal whether the energy landscapes of these bonds are similar.

Often a tether was formed between the two beads before the rupture event (Fig. 5). Because of the filamentous nature of the molecules, the tether may be formed of the PEVK fragment, the actin filament, or both. We argue, for the following reasons, that the tethers were formed mainly of the PEVK fragments. First, the lengths were most frequent within the range of the calculated fragment lengths (Fig. 5, *c* and *d*). Second, the persistence length of the tethers within the fragment-length range, calculated from wormlike-chain fits (28), was ~1 nm, which correlates well with previous mechanical measurements, using AFM, on PEVK molecules (32,34,35). By contrast, the persistence length of actin filaments is in the order of ~1 μm (36). However, in the case of the occasional tethers lengths exceeding the calculated lengths, a long-persistence-length segment was also present, which probably corresponds to the actin filament. In these

cases a likely arrangement is that the PEVK fragment interacted with a loop of F-actin or an actin-filament segment that broke loose from the HMM-coated bead surface.

The wide range of tether lengths observed indicates that F-actin can bind indiscriminately along the contour of the PEVK fragments. The lack of canonical actin-binding sites (37), the intrinsically disordered nature of the PEVK domain (5,6), and the indiscriminate actin-binding properties suggest that the domain may behave as a promiscuous actin-binding partner. We found a difference in the shape of tether-length distribution for polyE and PPAK (Fig. 5, *c* and *d*). The difference may be related to the accessibility of actin-binding regions in these fragments. PolyE, with its preponderance of negative charges, may acquire a more extended conformation than the PPAK fragment. In support of this idea, preliminary experiments with single-molecule AFM indicate that the persistence length of polyE (~0.9 nm) exceeds that of PPAK (~0.6 nm) (data not shown). As a consequence, the entire length of polyE may be more accessible for actin-binding than that of PPAK. In addition, because of the polyelectrolyte nature of polyE, its binding to F-actin may be tuned according to the local ionic strength.

Large stretches of the PEVK domain, such as the PEVKII fragment, contain numerous polyE and PPAK motifs arranged in series. Because of the putative random structure of the domain and its promiscuous binding to actin, it is difficult to predict the exact number of interactions with an actin filament. Under mechanical load the numerous interactions are broken sequentially as a function of time, resulting in stress relaxation (Fig. 5 *f*). Stress relaxation is a known feature of relaxed muscle and has been attributed to titin domain unfolding (38), PEVK-actin interaction (12), and interactions within the PEVK domain (39). Our results support the idea that the dynamics of PEVK-actin interaction play an important role in the stress-relaxation of striated muscle.

Possible physiological functions of the PEVK-actin interaction

The possible physiological role of the PEVK–F-actin interaction is most likely determined by the generated viscous load that resists the sliding movement of actin along the thick filament. In the absence of external force, the lifetime of the PEVK–F-actin bonds is high. The lifetime, at no force, of the polyE–F-actin bond, for example, is 223 s, which far exceeds the 67-s lifetime of the single-headed rigor bond between actin and myosin subfragment-1 (S-1) (29). Because of the energy landscape of the bonds, however, low forces (on the order of 10 pN) are sufficient to reduce the bond lifetime significantly. The long lifetimes of the PEVK–F-actin interaction in the absence of force suggest a structural function in the relaxed state of muscle. The interaction between the PEVK domain and actin may thus aid in preserving the structural integrity of the relaxed sarcomere. Because of isoform variation in PEVK and its interactions with additional thin-filament components (9), PEVK–thin filament interaction may be under fine control with yet-to-be discovered structural and functional consequences for the muscle sarcomere.

At changing sarcomere lengths (i.e., during contraction or extension), significant levels of viscous forces may be developed by the PEVK–F-actin interaction. Physiologically relevant sarcomeric filament-movement rates fall within the employed stretch rates (250–5000 nm/s). For example, in a cardiomyocyte contracting between sarcomere lengths of 1.7 and 2.2 μm with 80 beats/min, thin filaments slide past the thick filament (and hence titin) with a velocity of ~330 nm/s. Because of the geometry of the sarcomeric lattice, three PEVK domains are available to interact with each thin filament (40). If only one bond formed between each PEVK and the thin filament, then a force of ~30 pN/filament may be generated at the above loading rate. If, however, multiple bonds were formed, then the generated force may be far in excess of this level. Although easily overcome by the active force generated by actomyosin, which may be as large as ~1 nN/thin filament considering maximal isometric force (41,42) and the number of available myosin heads (43), the viscous force may be significant in modulating the mechanical behavior of striated muscle. Because a greater number of PEVK-actin bonds are likely to form during a more extended period spent in the relaxed state, the generated viscous forces are probably greater during the first contraction or stretch of the sarcomere. Therefore, PEVK-actin interaction might be important in determining thixotropy or strain softening in striated muscle (44,45). Whether PEVK–F-actin interaction plays a regulatory role during active contraction depends also on the on-rate of bond formation, which is yet unknown. Because the presence of PEVK fragments slows down the in vitro motility of actin filaments (14), such a regulatory role might also be possible.

We acknowledge the insightful discussions with Péter Tompa and the valuable comments of László Grama on the manuscript.

This work was supported by grants from the Hungarian Science Foundation (OTKA T049591), Hungarian National Office for Research and Technology (OMFB-01600/2006, OMFB-01627/2006, OMFB-00198/2007, KFKT-1-2006-0021), Hungarian Ministry of Health (ETT-506/2006), the Hungarian Ministry of Economy and Transport (GVOP-3.2.1.-2004-04-0226/3.0), the South Trans-Danubian Co-operative Research Center, and by the Howard Hughes Medical Institute.

REFERENCES

1. Granzier, H. L., and S. Labeit. 2004. The giant protein titin: a major player in myocardial mechanics, signaling, and disease. *Circ. Res.* 94: 284–295.
2. Tskhovrebova, L., and J. Trinick. 2003. Titin: properties and family relationships. *Nat. Rev. Mol. Cell Biol.* 4:679–689.
3. Labeit, S., and B. Kolmerer. 1995. Titins: giant proteins in charge of muscle ultrastructure and elasticity. *Science.* 270:293–296.

4. Freiburg, A., K. Trombitas, W. Hell, O. Cazorla, F. Fougerousse, T. Centner, B. Kolmerer, C. Witt, J. S. Beckmann, C. C. Gregorio, H. Granzier, and S. Labeit. 2000. Series of exon-skipping events in the elastic spring region of titin as the structural basis for myofibrillar elastic diversity. *Circ. Res.* 86:1114–1121.
5. Tompa, P. 2002. Intrinsically unstructured proteins. *Trends Biochem. Sci.* 27:527–533.
6. Trombitás, K., M. Greaser, S. Labeit, J. P. Jin, M. Kellermayer, M. Helmes, and H. Granzier. 1998. Titin extensibility in situ: entropic elasticity of permanently folded and permanently unfolded molecular segments. *J. Cell Biol.* 140:853–859.
7. Ma, K., L. Kan, and K. Wang. 2001. Polyproline II helix is a key structural motif of the elastic PEVK segment of titin. *Biochemistry.* 40:3427–3438.
8. Greaser, M. 2001. Identification of new repeating motifs in titin. *Proteins.* 43:145–149.
9. Gutierrez-Cruz, G., A. H. Van Herdeen, and K. Wang. 2001. Modular motif, structural folds and affinity profiles of the PEVK segment of human fetal skeletal muscle titin. *J. Biol. Chem.* 276:7442–7449.
10. Ma, K., and K. Wang. 2003. Malleable conformation of the elastic PEVK segment of titin: non-cooperative interconversion of polyproline II helix, beta turn and unordered structures. *Biochem. J.* 374:687–695.
11. Kulke, M., S. Fujita-Becker, E. Rostkova, C. Neagoe, D. Labeit, D. J. Manstein, M. Gautel, and W. A. Linke. 2001. Interaction between PEVK-titin and actin filaments: origin of a viscous force component in cardiac myofibrils. *Circ. Res.* 89:874–881.
12. Linke, W. A., M. Kulke, H. Li, S. Fujita-Becker, C. Neagoe, D. J. Manstein, M. Gautel, and J. M. Fernandez. 2002. PEVK domain of titin: an entropic spring with actin-binding properties. *J. Struct. Biol.* 137:194–205.
13. Yamasaki, R., M. Berri, Y. Wu, K. Trombitas, M. McNabb, M. S. Kellermayer, C. Witt, D. Labeit, S. Labeit, M. Greaser, and H. Granzier. 2001. Titin-actin interaction in mouse myocardium: passive tension modulation and its regulation by calcium/S100A1. *Biophys. J.* 81:2297–2313.
14. Nagy, A., P. Cacciafesta, L. Grama, A. Kengyel, A. Malnasi-Csizmadia, and M. S. Kellermayer. 2004. Differential actin binding along the PEVK domain of skeletal muscle titin. *J. Cell Sci.* 117:5781–5789.
15. Niederlander, N., F. Raynaud, C. Astier, and P. Chaussepied. 2004. Regulation of the actin-myosin interaction by titin. *Eur. J. Biochem.* 271:4572–4581.
16. Raynaud, F., C. Astier, and Y. Benyamin. 2004. Evidence for a direct but sequential binding of titin to tropomyosin and actin filaments. *Biochim. Biophys. Acta.* 1700:171–178.
17. Pardee, J. D., and J. A. Spudich. 1982. Purification of muscle actin. *Methods Enzymol.* 85:164–182.
18. Margossian, S. S., and S. Lowey. 1982. Preparation of myosin and its subfragments from rabbit skeletal muscle. *Methods Enzymol.* 85:55–72.
19. Kron, S. J., Y. Y. Toyoshima, T. Q. Uyeda, and J. A. Spudich. 1991. Assays for actin sliding movement over myosin-coated surfaces. *Methods Enzymol.* 196:399–416.
20. Howard, J., A. J. Hudspeth, and R. D. Vale. 1989. Movement of microtubules by single kinesin molecules. *Nature.* 342:154–158.
21. Sakakibara, H., H. Kojima, Y. Sakai, E. Katayama, and K. Oiwa. 1999. Inner-arm dynein c of *Chlamydomonas* flagella is a single-headed processive motor. *Nature.* 400:586–590.
22. Svoboda, K., and S. M. Block. 1994. Force and velocity measured for single kinesin molecules. *Cell.* 77:773–784.
23. Kellermayer, M. S. Z., S. B. Smith, H. L. Granzier, and C. Bustamante. 1997. Folding-unfolding transitions in single titin molecules characterized with laser tweezers. *Science.* 276:1112–1116.
24. Smith, S. B., Y. Cui, and C. Bustamante. 1996. Overstretching B-DNA: the elastic response of individual double-stranded and single-stranded DNA molecules. *Science.* 271:795–799.
25. Smith, S. B., Y. Cui, and C. Bustamante. 2003. Optical-trap force transducer that operates by direct measurement of light momentum. *Methods Enzymol.* 361:134–162.
26. Bell, G. I. 1978. Models for the specific adhesion of cells to cells. *Science.* 200:618–627.
27. Evans, E., and K. Ritchie. 1997. Dynamic strength of molecular adhesion bonds. *Biophys. J.* 72:1541–1555.
28. Bustamante, C., J. F. Marko, E. D. Siggia, and S. Smith. 1994. Entropic elasticity of lambda-phage DNA. *Science.* 265:1599–1600.
29. Nishizaka, T., R. Seo, H. Tadakuma, K. Kinosita, Jr., and S. Ishiwata. 2000. Characterization of single actomyosin rigor bonds: Load dependence of lifetime and mecahnical properties. *Biophys. J.* 79:962–974.
30. Tsuda, Y., H. Yasutake, A. Ishijima, and T. Yanagida. 1996. Torsional rigidity of single actin filaments and actin–actin bond breaking force under torsion measured directly by in vitro micromanipulation. *Proc. Natl. Acad. Sci. USA.* 93:12937–12942.
31. Forbes, J. G., A. J. Jin, G. Gutierrez-Cruz, W. L. Tsai, and K. Wang. 2005. Titin PEVK segment: charge-driven elasticity of the open and flexible polyampholyte. *J. Muscle Res. Cell Motil.* 26:291–301.
32. Nagy, A., L. Grama, T. Huber, P. Bianco, K. Trombitás, H. L. Granzier, and M. S. Z. Kellermayer. 2005. Hierarchical extensibility in the PEVK domain of skeletal-muscle titin. *Biophys. J.* 89:329–336.
33. Merkel, R., P. Nassoy, A. Leung, K. Ritchie, and E. Evans. 1999. Energy landscapes of receptor-ligand bonds explored with dynamic force spectroscopy. *Nature.* 397:50–53.
34. Li, H., A. F. Oberhauser, S. D. Redick, M. Carrion-Vazquez, H. P. Erickson, and J. M. Fernandez. 2001. Multiple conformations of PEVK proteins detected by single-molecule techniques. *Proc. Natl. Acad. Sci. USA.* 98:10682–10686.
35. Watanabe, K., P. Nair, D. Labeit, M. S. Kellermayer, M. Greaser, S. Labeit, and H. Granzier. 2002. Molecular mechanics of cardiac titin's PEVK and N2B spring elements. *J. Biol. Chem.* 277:11549–11558.
36. Gittes, F., B. Mickey, J. Nettleton, and J. Howard. 1993. Flexural rigidity of microtubules and actin filaments measured from thermal fluctuations in shape. *J. Cell Biol.* 120:923–934.
37. Van Troys, M., J. Vandekerckhove, and C. Ampe. 1999. Structural modules in actin-binding proteins: towards a new classification. *Biochim. Biophys. Acta.* 1448:323–348.
38. Minajeva, A., M. Kulke, J. M. Fernandez, and W. A. Linke. 2001. Unfolding of titin domains explains the viscoelastic behavior of skeletal myofibrils. *Biophys. J.* 80:1442–1451.
39. Trombitas, K., Y. Wu, M. McNabb, M. Greaser, M. S. Kellermayer, S. Labeit, and H. Granzier. 2003. Molecular basis of passive stress relaxation in human soleus fibers: assessment of the role of immunoglobulin-like domain unfolding. *Biophys. J.* 85:3142–3153.
40. Liversage, A. D., D. Holmes, P. J. Knight, L. Tskhovrebova, and J. Trinick. 2001. Titin and the sarcomere symmetry paradox. *J. Mol. Biol.* 305:401–409.
41. Piazzesi, G., L. Lucii, and V. Lombardi. 2002. The size and speed of the working sktroke for myosin and its dependence on the force. *J. Physiol.* 545:145–151.
42. Takagi, Y., E. Homsher, Y. E. Goldman, and H. Shuman. 2006. Force generation in single conventional actomyosin complexes under high dynamic load. *Biophys. J.* 90:1295–1307.
43. Suzuki, M., H. Fujita, and S. Ishiwata. 2005. A new muscle contractile system composed of a thick-filament lattice and a single actin filament. *Biophys. J.* 89:321–328.
44. Mutungi, G., and K. W. Ranatunga. 1996. The viscous, viscoelastic and elastic characteristics of resting fast and slow mammalian (rat) muscle fibres. *J. Physiol.* 496:827–836.
45. Whitehead, N. P., J. E. Gregory, D. L. Morgan, and U. Proske. 2001. Passive mechanical properties of the medial gastrocnemius muscle of the cat. *J. Physiol.* 536:893–903.